

Conformational variability of loops in the SARS-CoV-2 spike protein

Samuel W.K. Wong* and Zongjun Liu

Department of Statistics and Actuarial Science, University of Waterloo

May 3, 2021

Abstract

The SARS-CoV-2 spike (S) protein facilitates viral infection, and has been the focus of many structure determination efforts. This paper studies the conformations of loops in the S protein based on the available Protein Data Bank (PDB) structures. Loops, as flexible regions of the protein, are known to be involved in binding and can adopt multiple conformations. We identify the loop regions of the S protein, and examine their structural variability across the PDB. While most loops had essentially one stable conformation, 17 of 44 loop regions were observed to be structurally variable with multiple substantively distinct conformations. Loop modeling methods were then applied to the S protein loop targets, and loops with multiple conformations were found to be more challenging for the methods to predict accurately. Sequence variants and the up/down structural states of the receptor binding domain were also considered in the analysis.

Key words and phrases: COVID-19, loop modeling, conformational ensembles, decoy selection, sequence variants, protein structure prediction

1 Introduction

The COVID-19 disease is caused by the SARS-CoV-2 strain of coronavirus and its continued spread remains a concern since the first reported infections in late 2019 (Zhu et al., 2020). The SARS-CoV-2 viral genome encodes for four main structural proteins: spike, envelope, membrane, and nucleocapsid (Jiang et al., 2020). The spike (S) protein is of particular importance as it facilitates viral entry into host cells via its receptor binding domain (RBD), which recognizes human angiotensin-converting enzyme 2 (ACE2, Shang et al., 2020). Current vaccines being administered (e.g., Polack et al., 2020) achieve efficacy against SARS-CoV-2 by enabling the human body to

*Address for correspondence: Department of Statistics and Actuarial Science, University of Waterloo, Waterloo, ON, Canada. E-mail: samuel.wong@uwaterloo.ca

produce a modified version of its S protein; this in turn induces the production of neutralizing antibodies against the disease (Sewell et al., 2020).

Towards the development of such therapeutic interventions, many structure determination efforts have focused on the S protein, with the first standalone experimental structure of the full-length S protein obtained via cryo-electron microscopy in mid-February 2020 (Wrapp et al., 2020). Soon thereafter, the structure of the S protein RBD bound in a complex with ACE2 was also determined (Lan et al., 2020). As of January 13th, 2021, there were 203 structures deposited in the Protein Data Bank (PDB, Berman et al., 2000) associated with the SARS-CoV-2 S protein. These include studies of the standalone S protein (e.g., Cai et al., 2020), the S protein interacting with potential antibodies (e.g., Shi et al., 2020; Schoof et al., 2020), and the S protein interacting with various forms of ACE2 (e.g., Guo et al., 2021). Finally, with the emergence of S protein sequence variants, structures corresponding to mutations are also being studied, with D614G being a common example (Yurkovetskiy et al., 2020). While individual PDB structures generally provide static snapshots of protein conformations, it is well-known that proteins exhibit dynamic movement (Mittermaier and Kay, 2006; Henzler-Wildman and Kern, 2007). For the SARS-CoV-2 S protein, a well-documented example is the ability of its RBD to adopt ‘up’ (or open) and ‘down’ (or closed) states, where the ‘up’ state is the conformation capable of binding to ACE2 (Wrapp et al., 2020). Overall then, the PDB is a rich source of data for examining the conformational variability of the S protein, given the number of times its structure has been solved experimentally.

This paper focuses on the loop conformations of the S protein. Protein loops are the flexible connecting regions between regular secondary structures, and are often involved in the binding functionality of the protein (Fiser et al., 2000). For example, an extended loop of the SARS-CoV-2 S protein RBD interacts directly with loops of ACE2, as evidenced by the PDB structure of the RBD-ACE2 complex (Yan et al., 2020). Dynamic structural changes can occur both in larger regions of a protein (e.g., the SARS-CoV-2 RBD), as well as in individual loops adopting conformational rearrangements to carry out protein function in accordance with their environment (Papaleo et al., 2016). Thus, when a protein has been solved many times in the PDB, we may be able to observe distinct conformations among some of its loops in the recorded structures. In particular for the SARS-CoV-2 S protein, the PDB also documents sequence variants arising from mutations to some of its loop regions (e.g., Zhang et al., 2021), and the possible structural impacts of mutations can also be studied more broadly via computational methods (Chen et al., 2020; Sedova et al., 2020; Wong, 2020). Mutations to the S protein are especially of concern as they can lead to more infectious variants of SARS-CoV-2 (Li et al., 2020).

The task of structure prediction for flexible loops with multiple distinct conformations has been found to be more challenging than for rigid or inflexible ones (Marks et al., 2018). Most loop prediction methods are designed to identify the most likely conformation, e.g., with the lowest potential energy (Soto et al., 2008; Stein and Kortemme, 2013; Liang et al., 2014; Tang et al., 2014; Wong et al., 2017; Marks et al., 2017). Such methods are typically trained on loop sets where a single

conformation for each loop is taken from the PDB and assumed to represent the ground truth (Fiser et al., 2000), and thus tend to be more successful at accurately predicting inflexible loops with one ‘correct’ solution. Accuracy is typically measured by computing the root-mean-squared deviation (RMSD) of the backbone atoms from the predicted loop conformation to the corresponding one in the PDB. In order to study loops that can adopt multiple conformations, prediction methods might instead be applied to generate an ensemble of decoys, which often involves a combination of sampling and scoring steps (Barozet et al., 2021). Then, the success of different methods could be assessed on the basis of whether their generated ensembles include decoys that are close to each of the known conformations (Marks et al., 2018). For the SARS-CoV-2 S protein, this kind of assessment is a good test on the ability of current methods to explore a range of likely conformations, especially if further mutations were to occur in the flexible loop regions.

These considerations motivate the main contributions of this paper. First, we identify the loop regions from the known PDB structures of the SARS-CoV-2 S protein, and classify each loop according to whether it has been observed to adopt multiple distinct conformations or a single conformation only. We also note whether each loop has any sequence variants in the PDB, as these might be associated with structural changes. Second, we apply four current loop prediction methods on the identified loop regions, to generate ensembles of decoys for each one. Third, we discuss the results of these methods and the effectiveness of their application to modeling the loops of the S protein, along with the insights gained via our analyses.

2 Materials and Methods

2.1 Data preparation and selection of loop targets

The 3-D structures of the SARS-CoV-2 S protein were downloaded from the PDB at the RCSB website (<https://rcsb.org>) on January 13th, 2021, by navigating to the page in the ‘COVID-19 coronavirus resources’ section entitled ‘Spike proteins and receptor binding domains’. We extracted the S protein structures that are not bound to other molecules and have sequence length greater than 1000. This facilitates study of the S protein loop conformations within the context of a (mostly) full-length S protein structure, while without explicit interaction with other proteins. A total of 63 S protein PDB structures satisfied these criteria, most of which are provided as S protein trimers. We treated each chain as an individual sample and thus extracted a total of 193 S protein chains. Some realignments of the corresponding amino acid sequences were required in order to keep the residue numbers consistent across all chains; this was accomplished with the ClustalO service in Jalview (Waterhouse et al., 2009).

For each S protein chain, we first used DSSP (Kabsch and Sander, 1983) to determine the secondary structure classification of each residue. The 8-state DSSP classification was reduced to the traditional three types of helix (H), sheet (E), and coil (C) following the conventions in the

SPIDER3 (Heffernan et al., 2017) secondary structure prediction method: we map DSSP’s “G”, “H”, and “I” to H; “E” and “B” to E; the remaining three states are mapped to C. Due to structural variability, the classified type (H, E, or C) for a given residue position may not always agree among the 193 S protein chains. Thus, we define a loop region for our study as follows: a segment of five or more consecutive residues where over 50% of the protein chains at each position are classified as type C. Further, if two such segments are separated by only one E or H type residue (i.e., where less than 50% of the chains are type C at that position), we treat the two combined segments (including that connecting residue) as a single loop region.

With the starting and ending positions of loops defined in this manner, we check for the presence of sequence variants in each loop region among the S protein chains. If multiple distinct residue sequences are observed for a loop region, we shall treat each unique sequence separately for further analysis. This allows us to document the possible impact of mutations on the loop conformations. Thus, we shall say that a loop instance consists of its starting and ending positions together with its unique residue sequence.

We then consider the structural variability of a given loop instance using the RMSD metric. Taking all chains that have no missing coordinates within the loop residues, we compute their pairwise RMSD matrix based on the loop’s backbone (N, C $_{\alpha}$, C, and O) atoms, where the RMSD calculation is applied after the backbone atoms of each loop pair are optimally superimposed. Based on that distance matrix, we apply hierarchical clustering with average linkage (UPGMA, Sokal, 1958), where following Marks et al. (2018) we use a distance cutoff of 1.5 Å to form distinct clusters of loop conformations. Each cluster then represents a group of S protein chains which have a similar conformation for that loop instance. We consider a loop instance to have multiple distinct conformations if this step results in two or more such clusters of conformations; otherwise, we say that loop instance essentially adopts only a single conformation. Finally, we select a representative from each cluster by taking the chain with the highest structure resolution. If all of the chains in the cluster have poor structure resolution (> 3 Å), we remove that cluster from further analysis as the atomic coordinates are unlikely to be sufficiently reliable for making detailed structural comparisons.

Our full list of S protein loop targets for study thus consists of all the cluster representatives obtained from the above steps.

2.2 Loop modeling methods

To study the conformational variability of the identified S protein loop targets, we make use of several loop modeling methods. We focus on methods that incorporate sampling-based techniques for loop construction, which are suitable for stochastically generating an ensemble of decoys that represent plausible conformations for a loop. We include Rosetta’s next-generation KIC (NGK) algorithm (Stein and Kortemme, 2013), the DiSGro algorithm (Tang et al., 2014), and the PETALS algorithm (Wong et al., 2017), which are *ab initio* methods that explore the conformational space

with the guidance of an energy or scoring function; these do not directly make use any structure templates of known loop conformations. We also include the Sphinx algorithm (Marks et al., 2017), which is a hybrid method that begins with loop structure fragments obtained from sequence alignment and then completes the loop construction by *ab initio* sampling.

Using each of the methods, we generate an ensemble of 500 decoys for each loop target. The input structure is the loop target’s representative PDB chain, prepared by removing the coordinates of the loop residues: following loop modeling conventions, we treat the backbone atoms from the starting residue’s C atom to the ending residue’s C_α atom as unknown. The generated decoys are compared with each known conformation for that loop region, using the representative PDB chains identified in section 2.1. The backbone RMSD is used as the metric for comparison. For loop regions with multiple conformations or mutations present, we superimpose the backbone atoms of the starting and ending loop residues from the different representative PDB chains before computing the RMSD. Also note that for such loop regions, decoy generation is carried out multiple times, once using each representative PDB as input; taken together, we may thus assess whether decoys generated from different PDB inputs have good coverage of the conformational space for that loop region, including when mutations are present.

The scoring function associated with each method provides a ranking of its 500 generated decoys for a loop target. Thus, it is of interest to assess how well each method’s top-ranking decoys can predict the possible conformations of the loop region. We use three RMSD statistics for this purpose: (a) lowest RMSD among the 500 decoys, (b) RMSD of the top-ranked decoy, (c) lowest RMSD among the top-five ranked decoys. The first RMSD statistic evaluates the method according to its ability to construct native-like conformations, without regard to whether its scoring function can select the best prediction. The second RMSD statistic corresponds to typical loop modeling assessment, where the top-ranked decoy is selected as the prediction. However, this approach of selecting a single prediction would be less informative if the loop region has multiple conformations. Thus, we also use the third RMSD statistic: by selecting multiple (i.e., the top five) decoys, we can examine whether these top-ranking decoys are structurally distinct and accurately represent the different known conformations.

We close this section by briefly describing how each of the loop modeling methods are run. The NGK algorithm (Stein and Kortemme, 2013) is included in the Rosetta protein modeling suite (<https://www.rosettacommons.org/>), and we used the version provided in Rosetta release 2020.50 on December 18, 2020. NGK improves on a previous kinematic closure method, which consists of local conformational sampling and Monte Carlo minimization steps performed over two (coarse and full-atom) stages. The program outputs the lowest energy loop structure found in each run, and so to obtain the desired ensemble of decoys we ran the program 500 times, following the recommended settings in the online guide (https://guybrush.ucsf.edu/benchmarks/benchmarks/loop_modeling). The DiSGro algorithm (Tang et al., 2014) uses a distance-guided sequential chain-growth method to stochastically sample loop structures. We ran the authors’ program to generate

100,000 conformations for the best possible coverage of the conformational space, then used their scoring function to select the 500 decoys with the lowest energy. The PETALS algorithm (Wong et al., 2017) uses a sequence of propagation and filtering steps to explore the conformational space and locate low-energy structures. We ran the authors’ program with 60,000 seeds and outputted 30,000 decoys, then used an updated scoring function to select the 500 top-ranked decoys, see Appendix A for details. The Sphinx algorithm (Marks et al., 2017) begins by searching a database for suitable fragments according to loop sequence alignments; loop decoy backbones are then constructed by sampling and ranked with a coarse-grained energy function, after which side chains are added and SOAP-Loop (Dong et al., 2013) is used to obtain the final ranking of decoys. Sphinx is hosted on the SAbPred server (Dunbar et al., 2016), for which we automated the loop target submissions and used the “general protein” option; no PDB blacklist was necessary as the fragment database had not yet been updated to contain any COVID-19 S protein structures.

3 Results and discussion

3.1 Loop targets of the SARS-CoV-2 S protein

Applying the procedures in section 2.1 to the 193 standalone S protein chains, a total of 44 loop regions were identified in the SARS-CoV-2 S protein. Their starting and ending residue positions are listed in the first column of Table 1. Thirty-two of the 44 loops lie within the S1 subunit, with 13 in the N-terminal domain and 11 in the RBD; e.g., loops 475–487 and 495–506 have been previously noted to form contacts with ACE2 during binding (Ali and Vijayan, 2020). Loop sequences are shown in the second column of Table 1. Overall, there are five loop regions with sequence variants in the PDB: 380–394, 410–416, 600–608, 614–620, and 891–897. For these loop regions, the most common variant in the PDB is shown first, followed by the other variants which have their mutated residue indicated in bold. The mutation that has received the most attention thus far is D614G (e.g., Yurkovetskiy et al., 2020; Grubaugh et al., 2020; Zhang et al., 2020). Overall then, there are 50 loop instances, i.e., the combination of a loop’s residue positions and unique amino acid sequence.

The third column of Table 1 shows the number of PDB chains that contain a complete backbone for each loop instance. The final column lists the representative PDB chains for each loop instance, obtained by hierarchical clustering as described in section 2.1. Thus, for example, there are 170 S protein chains that contain the loop at positions 130–140; among these, three distinct conformations were found after clustering according to pairwise RMSD, among structures with resolution 3 Å or better; the PDB chains with the best resolution in each cluster were used to represent each conformation, namely 6xluA, 7kdkC, and 7kdIA. We illustrate this 130–140 loop example in the top panels of Figure 1: a histogram of all pairwise RMSDs of the loop backbone (among the 170 S protein chains that contain this loop) is shown on the left, while a close-up of the part of the S protein

Table 1: SARS-CoV-2 S protein loops. The first column shows the starting and ending positions of each identified loop region. The second column shows the loop sequences; if there are sequence variants in the PDB, the most common variant is listed first, and other variants have their mutated residues marked in bold. The number of PDB chains containing that loop instance are shown in the third column. The rightmost column lists the representative PDB chains (required to be 3 Å resolution or better) for each loop instance; if a loop instance has multiple conformations, each chain listed represents one distinct conformation.

Region	Sequence	#Chains	Representative conformations
14-27	QCVNLTTRTQLPPA	38	6zgeA, 7df3A
31-46	SFTRGVYYYPDKVFRSS	187	6xluA
56-60	LPFFS	187	6xluA
66-83	HAIHVSGTNGTKRFDNPV	11	none (all PDBs > 3Å resolution)
108-116	TTLDSKTQS	171	6xluA
130-140	VCEFQFCNDPF	170	6xluA, 7kdkC, 7kdIA
146-168	HKNNKSWMESEFRVYSSANNCTF	40	6zgeA, 7df3A
172-187	SQPFLMDLEGKQGFK	54	6zgeA, 6zoxA
210-222	INLVRDLPQGFSA	156	6xluA
230-236	PIGINIT	187	6xluA
245-263	HRSYLTPGDSSSGWTAGAA	26	6zgeA
280-284	NENGT	187	6xluA
304-310	KSFTVEK	187	6xluA
320-324	VQPTE	187	6xluA, 6xm0A
329-338	FPNITNLCPP	182	6xluA, 6xm0B
343-348	NATRFA	183	6xluA
370-375	NSASFS	184	6xluA, 6zgeA
380-394	YGVSPTKLNDLCFTN	172	6xluA
	YGVCPTKLNDLCFTN	12	6x29A
410-416	IAPGQTG	181	6xluA
	IAPCQTG	3	6zoxA
422-430	NYKLPDDFT	184	6xluA, 6xm0B
438-451	SNNLDSKVGGNYYN	95	6zgeA, 7kdIB
454-472	RLFRKSNLKPFRDISTEI	98	6xluA
475-487	AGSTPCNGVEGFN	94	6xluA, 6xm0B
495-506	YGFQPTNGVGYQ	127	6xluA, 6xm0B, 7kdIB
517-523	LLHAPAT	171	6xluA, 6xm0A, 6xm0B, 6xm3A
526-537	GPKKSTNLVKNK	184	6xluA
555-564	SNKKFLPFQQ	188	6xluA
578-583	DPQTLE	188	6xluA
600-608	PGTNTSNQV	176	6xluA
	PGTNTSNEV	12	none (all PDBs > 3Å resolution)
614-620	DVNCTEV	106	6xluA
	G VNCTEV	42	7kdkA
	N VNCTEV	6	7a4nA
624-641	IHADQLTPTWRVYSTGSN	26	6xluA
656-663	VNNSYECD	188	6xluA
697-710	MSLGAENSVAYSNN	188	6xluA
783-816	AQVKQIYKTPPIKDFGGFNFSQILPDPSKPSKRS	147	6xluA
825-836	KVTLADAGFIKQ	39	6xluB, 6xm0B, 6xm3C, 6zgeA
841-848	LGDIAARD	43	6xluA, 6xm0B, 6xm4B, 6zgeA, 7df3A
862-866	PPLLT	188	6xluA
891-897	GAALQIP	179	6xluA
	G PALQIP	9	7a4nA
908-913	GIGVTQ	188	6xluA
968-976	SNFGAISSV	191	6xluA, 6xraA
1033-1046	VLGQSKRVDFCGKG	191	6xluA
1106-1112	QRNFYEP	191	6xluA
1124-1132	GNCDDVIGI	191	6xluA, 6xraA
1135-1141	NTVYDPL	164	6xluA, 6xraA

chain containing the loop is shown on the right. The histogram shows that there were many pairs of chains with loop RMSD $> 2 \text{ \AA}$ and clustering identified the three distinct conformations colored in red, blue, and turquoise. In contrast, the bottom panels of Figure 1 show a loop example (555–564) with little structural variability: the pairwise RMSDs do not exceed around 1.5 \AA and clustering identified just one main conformation (colored in red). Overall, there were two loop instances with sparse structural information, where no high resolution structures were available: 66–83 and 600–608 with the Q607E mutation. Notably, of the 48 loop instances where $\leq 3 \text{ \AA}$ resolution structures were available, 17 of these had multiple distinct conformations, and seven of these 17 were located within the RBD.

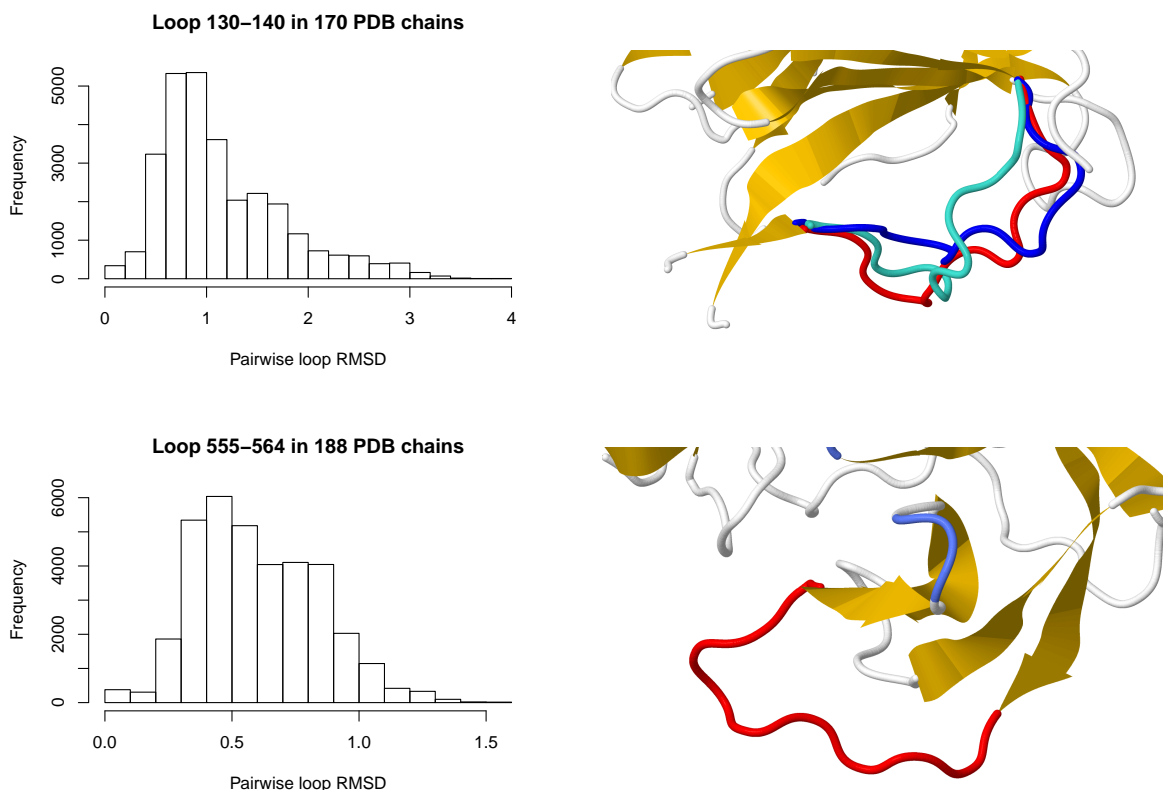


Figure 1: Two examples of SARS-CoV-2 S protein loops: 130–140 (top panels) and 555–564 (bottom panels). The histograms (left panels) shows the pairwise RMSDs of the loop backbone among all S protein chains containing that loop: it can be seen that 130–140 exhibits higher structural variability than 555–564. The right panels display close-ups of the representative loop conformations: 130–140 has three distinct conformations, colored in red, blue, and turquoise; 555–564 has essentially one conformation, colored in red.

It is well-known that the SARS-CoV-2 RBD as a whole can adopt an ‘up’ or ‘down’ conformational state (Wrapp et al., 2020). Thus, we examined whether this higher propensity for multiple conformation loops within the RBD might be associated with the chains having an ‘up’ or ‘down’ RBD state, even when the S protein chain is considered in isolation. Notably, both 475–487 and 495–506 which interact with ACE2 are among these. We took PDB 6zge (Wrobel et al., 2020),

where it is known that chain A has a ‘down’ RBD and chain B has an ‘up’ RBD. Then, each of the 193 S protein chains was classified as ‘up’ or ‘down’ according to whether its backbone RMSD to 6zgeB or 6zgeA was smaller. Based on this criterion, the loop at 370–375 has both distinct conformations coming from ‘down’ RBD chains, while four other loops with two conformations (329–338, 422–430, 438–451, 475–487) indeed have one conformation associated with the ‘up’ state and the other associated with the ‘down’ state. Of the two remaining loops, 495–506 has one conformation from an ‘down’ RBD and two from an ‘up’ RBD, while 517–523 has two conformations from each. Overall then, five RBD loop regions have structures that do not vary significantly with the RBD state (370–375 and the four single conformation loops in the RBD), while the other six do potentially vary.

We next examined the five loop regions that had sequence variants present in the PDB. Taking the representative chain for each sequence variant listed in Table 1, we computed the loop backbone RMSD between the representatives and the results are shown in Table 2. For example, for the loop region 380–394, the sequence variants are S and C at position 383, represented by 6xluA and 6x29A respectively; these structures have backbone RMSD 1.15 Å computed on the loop residues. For the loop 600–608, there were no high resolution PDB structures containing the Q607E mutation, so for the comparison we used the best structure available (6vybA, at 3.2 Å resolution) as its representative. Overall, these particular sequence variants do not have large impacts on the loop conformations, with observed backbone differences all around 1 Å or less.

Table 2: Backbone RMSDs between the PDB chains representing the different sequence variants, in loop regions where mutations are present. RMSDs are computed on the loop residues only. The residues that differ between the sequence variants are highlighted in bold.

Region	Sequence 1	Sequence 2	RMSD
380-394	YGV S PTKLNDLCFTN	YGV C PTKLNDLCFTN	1.15
410-416	IAP G QTG	IAP C QTG	0.32
600-608	PGTNT S N Q V	PGTNT S NEV	0.29
614-620	D VNCTEV	G VNCTEV	0.85
614-620	D VNCTEV	N VNCTEV	0.88
614-620	G VNCTEV	N VNCTEV	0.55
891-897	GAAL Q IP	GPAL Q IP	0.18

In total, there are 74 representative conformations for the 50 loop instances, as listed in Table 1. Three of the loop instances were omitted from consideration for loop modeling, as all of their PDB chains were missing a residue immediately next to the loop: 14–27 (both conformations missing residue 13), 614–620 with the D614G and D614N mutations (both missing residue 621). Thus we used the loop modeling methods to study a total of 70 loop targets.

3.2 Loop modeling results

The four methods described in section 2.2 were applied to model the conformations of the 70 loop targets identified in section 3.1. Of these, 63 targets could be run successfully using all four methods. NGK and PETALS completed decoy generation for all 70 targets, while DiSGro completed 67 targets and Sphinx completed 63 targets. We focus the discussion on the results of the 63 loop targets for which all the methods could successfully generate decoys; the 7 remaining cases are discussed briefly at the end.

First, we consider the results of loop reconstruction, that is, each method’s ability to predict the original loop conformation in the PDB chain used as input for that loop target. This is the classic setup for assessing loop modeling methods: for example, there are three targets for the loop 130–140 corresponding to its three conformations, represented by 6xluA, 7kdkC, and 7dklA; the decoys generated using 6xluA were compared to the original loop conformation in 6xluA, and likewise for the other two targets. We categorized the targets according to whether they belong to loop instances having multiple conformations or not; these categories are denoted as ‘Multiple conf.’ and ‘Single conf.’ in Table 3, containing 37 and 26 loop targets respectively. Table 3 displays the three RMSD statistics described in the Materials and Methods section – lowest RMSD among the 500 decoys (column 3), RMSD of the top-ranked decoy (column 4), and lowest RMSD among the top-five ranked decoys (column 5) – averaged over the loop targets for each method. On average, all four methods can generate decoys at <2 Å from the native conformation. However, it remains difficult to correctly rank the generated decoys, with the RMSDs of the top-ranked decoy often substantially higher than the best decoy available. NGK is the most accurate at this task, achieving an average reconstruction accuracy of 2.74 Å over the 63 targets. When each method is allowed to choose five decoys, then it is more likely that at least one of the five is close to the native conformation; e.g., NGK’s average accuracy increases to 2.07 Å. Further, the difficulty of this loop reconstruction task appears to vary by target category: for all four methods, the RMSD averages for loops with multiple conformations are higher than for single conformation loops. Note that the loop targets in both categories have relatively similar lengths, averaging 9.6 residues long for ‘Single conf.’ and 10.0 residues long for ‘Multiple conf.’, so it is unlikely that the RMSD differences can be attributed to differences in loop lengths alone. This echos the finding in Marks et al. (2018), that loops with multiple conformations can be more difficult to predict. The detailed results for each target individually are given in Tables S1 (for single conformation targets) and S2 (for multiple conformation targets) of the Supporting Information.

Second, we consider the loop instances with multiple distinct conformations. Recall that for these loop instances, decoy generation is carried out once using each representative PDB as input. Taking the loop 130–140 for example: the decoys generated using 6xluA are compared to the conformations in each of 6xluA, 7kdkC, and 7dklA (after the loop anchors are optimally superimposed); the RMSD averaged over those three comparisons then provides the overall result for that loop target; the same is done using the decoys from 7kdkC and 7dklA. This assesses how well the decoys generated from an

Table 3: RMSD metrics for assessing the loop reconstruction accuracy of the four methods. The loop backbone RMSDs shown are averaged over single conformation targets ($n = 26$), multiple conformation targets ($n = 37$), and all targets ($n = 63$). The columns ‘Minimum’, ‘Top decoy’, and ‘Top 5 decoys’ refer respectively to the lowest RMSD among the 500 decoys, RMSD of the top-ranked decoy, and lowest RMSD among the top-five ranked decoys.

		Loop backbone RMSD		
Method	Target category	Minimum	Top decoy	Top 5 decoys
DiSGro	Single conf.	1.26	3.00	1.96
	Multiple conf.	1.81	4.84	3.68
	All	1.59	4.08	2.97
NGK	Single conf.	0.83	1.98	1.45
	Multiple conf.	1.47	3.27	2.50
	All	1.20	2.74	2.07
PETALS	Single conf.	1.28	2.25	1.72
	Multiple conf.	1.75	3.75	2.82
	All	1.55	3.13	2.36
Sphinx	Single conf.	1.35	3.96	2.92
	Multiple conf.	1.88	4.82	3.60
	All	1.66	4.46	3.32

individual PDB input can reproduce all the known conformations for that loop instance. The results are summarized in Table 4 using the same three RMSD metrics, averaged over the targets in the multiple conformation category. This task is noticeably more challenging, as evidenced by RMSDs in Table 4 which are all larger than the corresponding values in the ‘Multiple conf.’ rows of Table 3 for all four methods. While the ‘Top decoy’ RMSDs are expected to be increase relative to Table 3, a similar increase still occurs when taking the entire decoy set (‘Minimum’ column, e.g., 1.47 to 2.29 Å for NGK) and when allowing methods to choose the top five decoys (‘Top 5 decoys’ column, e.g., 2.50 to 3.46 Å for NGK). This suggests that building the loop using the atomic environment in a specific PDB chain may preclude the methods from being able to locate and predict all the possible loop conformations. The detailed results for each loop target individually are given in Table S3 of the Supporting Information.

Third, we examine the multiple conformation loop instances in the RBD. Since it was noted in section 3.1 that the ‘up’ or ‘down’ RBD state may be associated with conformation changes for up to six of the RBD loop regions, of interest is whether modeling these loops in the RBD is also more challenging. The RMSD metrics for these multiple conformation RBD loops are presented in Table 5, which are calculated in the same way as Table 4 but averaged over the subset of loop targets in the RBD. The RMSD values in Tables 4 and 5 are of similar magnitude, indicating that the difficulty of the RBD loop targets are not noticeably different from other multiple conformation targets. The average length of these loop targets in the RBD is 9.9 residues, and similar to the average length (10.0) among all multiple conformation targets.

Fourth, we comment briefly on the loop regions with sequence variants in the PDB. These

Table 4: RMSD metrics for the loop instances with multiple conformations. The loop backbone RMSDs shown are averaged over the targets in the multiple conformation category, where decoys generated from each target are compared to all known conformations for that loop instance. The columns ‘Minimum’, ‘Top decoy’, and ‘Top 5 decoys’ refer respectively to the lowest RMSD among the 500 decoys, RMSD of the top-ranked decoy, and lowest RMSD among the top-five ranked decoys.

Loop backbone RMSD			
Method	Minimum	Top decoy	Top 5 decoys
DiSGro	2.56	5.42	4.38
NGK	2.29	4.22	3.46
PETALS	2.60	4.43	3.57
Sphinx	2.44	5.35	4.23

Table 5: RMSD metrics for the loop instances in the RBD with multiple conformations. The loop backbone RMSDs shown are averaged over the targets in the multiple conformation category within the RBD, where decoys generated from each target are compared to all known conformations for that loop instance. The columns ‘Minimum’, ‘Top decoy’, and ‘Top 5 decoys’ refer respectively to the lowest RMSD among the 500 decoys, RMSD of the top-ranked decoy, and lowest RMSD among the top-five ranked decoys.

Loop backbone RMSD			
Method	Minimum	Top decoy	Top 5 decoys
DiSGro	2.13	5.32	4.40
NGK	2.04	4.25	3.39
PETALS	2.51	4.37	3.27
Sphinx	2.14	5.37	4.16

particular mutations were found (see Table 2) to have little impact on the corresponding loop structures. Thus, these examples were not expected to pose additional challenges for the loop modeling methods. Indeed, for these loop regions, we found that the decoys generated from one sequence variant could be used to reasonably predict the loop conformation for the other variant(s). Detailed results for each sequence variant are given in Table S4 of the Supporting Information.

Finally, we mention the challenges encountered when running the methods, which led to seven loop targets being omitted from the above analyses. The two very long loops in the set, namely 146–168 and 783–816, were particularly difficult, with DiSGro and Sphinx unable to generate decoys possibly due to their lengths. The 146–168 loop has two conformations, both of which could be reconstructed moderately well by PETALS (top decoy RMSDs: 3.13 for 6zgeA, 2.83 for 7df3A), and with lower accuracy by NGK (top decoy RMSDs: 3.84 for 6zgeA, 7.30 for 7df3A). The length 34 loop (783–816) is very challenging, and no method could give useful results (top decoy RMSDs: 23.8 for NGK, 14.6 for PETALS). The Sphinx webserver was also unable to generate decoys for 31–46, 320–324 (6xm0A conformation), 697–710, and 1135–1141, possibly due to a lack of suitable templates. Further, some of Sphinx’s jobs were unable to complete the full SOAP-Loop ranking steps; thus, we used the 500 SOAP-Loop ranked decoys if they were available, and otherwise selected

its top 500 decoys from the coarse-grained ranking stage for our analysis. Detailed results for the seven omitted targets are provided in Table S5 of the Supporting Information.

4 Conclusion

In this paper, we studied the conformations of loops in the SARS-CoV-2 S protein. We extracted all SARS-CoV-2 S protein loop regions, examined their sequence and structural variability based on the available structures in the PDB, and applied loop modeling methods to assess how well the loop conformations could be predicted. Forty-four loop regions were identified, and as the structure of the S protein has been experimentally solved many times, 17 loop instances were observed to have substantive structural variability and be able to adopt multiple distinct conformations. Some of these correspond to key loops that are known to be involved in binding. The structural impact of several sequence variants have also been documented in the PDB. We found that the structurally flexible loops with multiple conformations in the S protein were more challenging for loop modeling methods, than relatively inflexible loops with a single conformation. Loops in the key RBD were more likely to be flexible, but were not of increased difficulty for loop modeling. Overall, this work provides insight into the abilities of current loop prediction methods for a key protein associated with the ongoing COVID-19 disease, and identifies the loops where structural flexibility could play a role as the SARS-CoV-2 virus continues to evolve.

This work also noted some limitations of current loop prediction methods, most of which were designed to predict a single ‘correct’ conformation. Even when methods were allowed to pick multiple (i.e., top-five ranked) decoys, they were less successful at identifying the correct structures of loops that had multiple conformations. Finally, we note one limitation of this study, namely our focus on loops rather than more global protein structure. In this sense, more global structural variability across S protein chains may have hindered the ability of methods to locate all the distinct loop conformations from a single input structure, since the rest of the protein chain is held fixed. Additionally, we found the observable changes to loop structures from known sequence variants in the PDB to be small. There could be more global structural changes due to mutation not detected by the current analysis, for example the D614G mutation (Yurkovetskiy et al., 2020). Nonetheless, loops deserve careful study in their own right, due to their functional importance. Further study could focus on larger-scale variability in the S protein structure, leveraging the rich source of experimental data available in the PDB to better understand COVID-19.

Acknowledgements

This work was partially supported by Discovery Grant RGPIN-2019-04771 from the Natural Sciences and Engineering Research Council of Canada.

Data availability statement

The data that support the findings of this study are openly available in the RCSB Protein Data Bank.

A Updated scoring function for PETALS algorithm

In this work we also tested a strategy for improving the energy function accuracy of the PETALS algorithm, in its ability to rank generated loop decoys. The set of structures used for training is the same as that described in Wong et al. (2017), namely, the CulledPDB list by PISCES (Wang and Dunbrack Jr, 2003) on March 14, 2015 with maximum 20% sequence identity, resolution 2.0 Å, and R -factor cutoff 0.25, thus ensuring no SARS-CoV-2 S protein structures were present. Loop regions were extracted via DSSP, from which we compiled 10786 loops with lengths ranging from 5 to 10 residues.

The PETALS algorithm was first used to generate 200 decoys for each loop, and for each decoy we computed: RMSD to the native conformation, 210 distance-based energy terms corresponding to each pair of atom types defined in DiSGro’s energy function (Tang et al., 2014), and a backbone torsion term (Wong et al., 2017). We then define \hat{y}_{ij} as the predicted energy of the i -th loop’s j -th decoy according to

$$\hat{y}_{ij} = T_{ij} + \sum_{k=1}^{210} \beta_k E_{ijk},$$

where β_k ’s are coefficients associated with each energy term E_{ijk} to be trained, and T_{ij} is the torsion term. Then define the square-error loss function

$$\sum_{i=1}^N \sum_{j=1}^{200} w_{ij} (f(\hat{y}_{ij}) - f(\text{RMSD}_{ij}))^2, \quad (1)$$

where RMSD_{ij} is the RMSD to native and w_{ij} is the weight associated with the i -th loop’s j -th decoy, N is the number of training loops, and f is a mapping function associated with the rank of that decoy. The decoys with the lowest RMSDs are the ones that best resemble the true conformation; thus the goal is to train the β_k ’s to minimize this loss function so that the rankings of the predicted energies and the rankings of the RMSD values match as closely as possible.

We chose $f(\cdot)$ to be a function that maps values into quantile bins. Specifically, we ranked the 200 predicted energies $\{\hat{y}_{ij}\}_{j=1}^{200}$ from smallest to largest, then assigning $f = 1$ to the best 10%, $f = 2$ to the next 10%, until $f = 10$ for the last 10%. We ranked the 200 RMSD values $\{\text{RMSD}_{ij}\}_{j=1}^{200}$ and assigned values of f the same way. Positive weights w_{ij} were assigned to the top five quantile bins, with higher weights for the better ranked predicted energies: 1.0 for the best 10%, 0.9 for the next 10%, until 0.6 for 5th quantile bin, and zero for the rest. We used 80% of the loops as training data and 20% as validation data. As gradient information was unavailable due to the discrete nature

of the model, the PySwarms (Miranda, 2018) implementation of Particle Swarm Optimization was used to minimize the square error loss function in Equation (1).

References

- Ali, A. and Vijayan, R. (2020). Dynamics of the ace2–sars-cov-2/sars-cov spike protein interface reveal unique mechanisms. *Scientific reports*, 10(1):1–12.
- Barozet, A., Bianciotto, M., Vaisset, M., Simeon, T., Minoux, H., and Cortés, J. (2021). Protein loops with multiple meta-stable conformations: A challenge for sampling and scoring methods. *Proteins: Structure, Function, and Bioinformatics*, 89(2):218–231.
- Berman, H. M., Westbrook, J., Feng, Z., Gilliland, G., Bhat, T. N., Weissig, H., Shindyalov, I. N., and Bourne, P. E. (2000). The protein data bank. *Nucleic acids research*, 28(1):235–242.
- Cai, Y., Zhang, J., Xiao, T., Peng, H., Sterling, S. M., Walsh, R. M., Rawson, S., Rits-Volloch, S., and Chen, B. (2020). Distinct conformational states of sars-cov-2 spike protein. *Science*, 369(6511):1586–1592.
- Chen, J., Wang, R., Wang, M., and Wei, G.-W. (2020). Mutations strengthened sars-cov-2 infectivity. *Journal of Molecular Biology*, 432(19):5212–5226.
- Dong, G. Q., Fan, H., Schneidman-Duhovny, D., Webb, B., and Sali, A. (2013). Optimized atomic statistical potentials: assessment of protein interfaces and loops. *Bioinformatics*, 29(24):3158–3166.
- Dunbar, J., Krawczyk, K., Leem, J., Marks, C., Nowak, J., Regep, C., Georges, G., Kelm, S., Popovic, B., and Deane, C. M. (2016). Sabpred: a structure-based antibody prediction server. *Nucleic acids research*, 44(W1):W474–W478.
- Fiser, A., Do, R. K. G., and Šali, A. (2000). Modeling of loops in protein structures. *Protein science*, 9(9):1753–1773.
- Grubaugh, N. D., Hanage, W. P., and Rasmussen, A. L. (2020). Making sense of mutation: what d614g means for the covid-19 pandemic remains unclear. *Cell*, 182(4):794–795.
- Guo, L., Bi, W., Wang, X., Xu, W., Yan, R., Zhang, Y., Zhao, K., Li, Y., Zhang, M., Cai, X., et al. (2021). Engineered trimeric ace2 binds viral spike protein and locks it in “three-up” conformation to potentially inhibit sars-cov-2 infection. *Cell research*, 31(1):98–100.
- Heffernan, R., Yang, Y., Paliwal, K., and Zhou, Y. (2017). Capturing non-local interactions by long short-term memory bidirectional recurrent neural networks for improving prediction of protein

- secondary structure, backbone angles, contact numbers and solvent accessibility. *Bioinformatics*, 33(18):2842–2849.
- Henzler-Wildman, K. and Kern, D. (2007). Dynamic personalities of proteins. *Nature*, 450(7172):964–972.
- Jiang, S., Hillyer, C., and Du, L. (2020). Neutralizing antibodies against sars-cov-2 and other human coronaviruses. *Trends in immunology*, 41(5):355–359.
- Kabsch, W. and Sander, C. (1983). Dictionary of protein secondary structure - pattern-recognition of hydrogen-bonded and geometrical features. *Biopolymers*, 22(12):2577–2637.
- Lan, J., Ge, J., Yu, J., Shan, S., Zhou, H., Fan, S., Zhang, Q., Shi, X., Wang, Q., Zhang, L., et al. (2020). Structure of the sars-cov-2 spike receptor-binding domain bound to the ace2 receptor. *Nature*, 581(7807):215–220.
- Li, Q., Wu, J., Nie, J., Zhang, L., Hao, H., Liu, S., et al. (2020). The impact of mutations in sars-cov-2 spike on viral infectivity and antigenicity. *Cell*, 182(5):1284–1294.
- Liang, S., Zhang, C., and Zhou, Y. (2014). Leap: Highly accurate prediction of protein loop conformations by integrating coarse-grained sampling and optimized energy scores with all-atom refinement of backbone and side chains. *Journal of computational chemistry*, 35(4):335–341.
- Marks, C., Nowak, J., Klostermann, S., Georges, G., Dunbar, J., Shi, J., Kelm, S., and Deane, C. M. (2017). Sphinx: merging knowledge-based and ab initio approaches to improve protein loop prediction. *Bioinformatics*, 33(9):1346–1353.
- Marks, C., Shi, J., and Deane, C. M. (2018). Predicting loop conformational ensembles. *Bioinformatics*, 34(6):949–956.
- Miranda, L. J. V. (2018). PySwarms, a research-toolkit for Particle Swarm Optimization in Python. *Journal of Open Source Software*, 3.
- Mittermaier, A. and Kay, L. E. (2006). New tools provide new insights in nmr studies of protein dynamics. *science*, 312(5771):224–228.
- Papaleo, E., Saladino, G., Lambrughi, M., Lindorff-Larsen, K., Gervasio, F. L., and Nussinov, R. (2016). The role of protein loops and linkers in conformational dynamics and allostery. *Chemical reviews*, 116(11):6391–6423.
- Polack, F. P., Thomas, S. J., Kitchin, N., Absalon, J., Gurtman, A., Lockhart, S., Perez, J. L., Pérez Marc, G., Moreira, E. D., Zerbini, C., et al. (2020). Safety and efficacy of the bnt162b2 mrna covid-19 vaccine. *New England Journal of Medicine*, 383(27):2603–2615.

- Schoof, M., Faust, B., Saunders, R. A., Sangwan, S., Rezelj, V., Hoppe, N., Boone, M., Billesbølle, C. B., Puchades, C., Azumaya, C. M., et al. (2020). An ultrapotent synthetic nanobody neutralizes sars-cov-2 by stabilizing inactive spike. *Science*, 370(6523):1473–1479.
- Sedova, M., Jaroszewski, L., Alisoltani, A., and Godzik, A. (2020). Coronavirus3d: 3d structural visualization of covid-19 genomic divergence. *Bioinformatics*, 36(15):4360–4362.
- Sewell, H. F., Agius, R. M., Kendrick, D., and Stewart, M. (2020). Covid-19 vaccines: delivering protective immunity. *BMJ*, 371:m4838.
- Shang, J., Ye, G., Shi, K., Wan, Y., Luo, C., Aihara, H., Geng, Q., Auerbach, A., and Li, F. (2020). Structural basis of receptor recognition by sars-cov-2. *Nature*, 581(7807):221–224.
- Shi, R., Shan, C., Duan, X., Chen, Z., Liu, P., Song, J., Song, T., Bi, X., Han, C., Wu, L., et al. (2020). A human neutralizing antibody targets the receptor-binding site of sars-cov-2. *Nature*, 584(7819):120–124.
- Sokal, R. R. (1958). A statistical method for evaluating systematic relationships. *Univ. Kansas, Sci. Bull.*, 38:1409–1438.
- Soto, C. S., Fasnacht, M., Zhu, J., Forrest, L., and Honig, B. (2008). Loop modeling: Sampling, filtering, and scoring. *Proteins: Structure, Function, and Bioinformatics*, 70(3):834–843.
- Stein, A. and Kortemme, T. (2013). Improvements to robotics-inspired conformational sampling in rosetta. *PloS one*, 8(5).
- Tang, K., Zhang, J., and Liang, J. (2014). Fast protein loop sampling and structure prediction using distance-guided sequential chain-growth monte carlo method. *PLoS computational biology*, 10:e1003539.
- Wang, G. and Dunbrack Jr, R. L. (2003). Pisces: a protein sequence culling server. *Bioinformatics*, 19(12):1589–1591.
- Waterhouse, A. M., Procter, J. B., Martin, D. M., Clamp, M., and Barton, G. J. (2009). Jalview version 2—a multiple sequence alignment editor and analysis workbench. *Bioinformatics*, 25(9):1189–1191.
- Wong, S. W. (2020). Assessing the impacts of mutations to the structure of covid-19 spike protein via sequential monte carlo. *Journal of Data Science*, 18(3):511–525.
- Wong, S. W., Liu, J. S., and Kou, S. (2017). Fast de novo discovery of low-energy protein loop conformations. *Proteins: Structure, Function, and Bioinformatics*, 85(8):1402–1412.

- Wrapp, D., Wang, N., Corbett, K. S., Goldsmith, J. A., Hsieh, C.-L., Abiona, O., Graham, B. S., and McLellan, J. S. (2020). Cryo-em structure of the 2019-ncov spike in the prefusion conformation. *Science*, 367(6483):1260–1263.
- Wrobel, A. G., Benton, D. J., Xu, P., Roustan, C., Martin, S. R., Rosenthal, P. B., Skehel, J. J., and Gamblin, S. J. (2020). Sars-cov-2 and bat ratg13 spike glycoprotein structures inform on virus evolution and furin-cleavage effects. *Nature structural & molecular biology*, 27(8):763–767.
- Yan, R., Zhang, Y., Li, Y., Xia, L., Guo, Y., and Zhou, Q. (2020). Structural basis for the recognition of sars-cov-2 by full-length human ace2. *Science*, 367(6485):1444–1448.
- Yurkovetskiy, L., Wang, X., Pascal, K. E., Tomkins-Tinch, C., Nyalile, T. P., Wang, Y., Baum, A., Diehl, W. E., Dauphin, A., Carbone, C., et al. (2020). Structural and functional analysis of the d614g sars-cov-2 spike protein variant. *Cell*, 183(3):739–751.
- Zhang, J., Cai, Y., Xiao, T., Lu, J., Peng, H., Sterling, S. M., Walsh, R. M., Rits-Volloch, S., Zhu, H., Woosley, A. N., et al. (2021). Structural impact on sars-cov-2 spike protein by d614g substitution. *Science*.
- Zhang, L., Jackson, C. B., Mou, H., Ojha, A., Peng, H., Quinlan, B. D., Rangarajan, E. S., Pan, A., Vanderheiden, A., Suthar, M. S., et al. (2020). Sars-cov-2 spike-protein d614g mutation increases virion spike density and infectivity. *Nature communications*, 11(1):1–9.
- Zhu, N., Zhang, D., Wang, W., Li, X., Yang, B., Song, J., Zhao, X., Huang, B., Shi, W., Lu, R., et al. (2020). A novel coronavirus from patients with pneumonia in china, 2019. *New England journal of medicine*, 382:727–733.

Supporting Information for “Conformational variability of loops in the SARS-CoV-2 spike protein”

- Table S1: Detailed loop reconstruction accuracies of the four methods, for each of the single conformation targets.
- Table S2: Detailed loop reconstruction accuracies of the four methods, for each of the multiple conformation targets.
- Table S3: Detailed RMSD metrics for the loop instances with multiple conformations, comparing the decoys generated from a given target to all known conformations for that loop instance.
- Table S4: Detailed RMSD metrics for the loop regions with sequence variants.
- Table S5: Detailed RMSD metrics for the seven loop targets omitted from the main analysis.

Table S1: RMSD metrics for assessing the loop reconstruction accuracy of the four methods. The loop backbone RMSDs are shown for each of the 26 single conformation targets. The columns ‘Min.’, ‘Top1’, and ‘Top5’ refer respectively to the lowest RMSD among the 500 decoys, RMSD of the top-ranked decoy, and lowest RMSD among the top-five ranked decoys. ‘Region’ is the residue range of the loop, and ‘PDB’ indicates the representative chain for the loop conformation.

Region	PDB	DiSGro			NGK			PETALS			Sphinx		
		Min.	Top1	Top5	Min.	Top1	Top5	Min.	Top1	Top5	Min.	Top1	Top5
56-60	6xluA	0.19	0.62	0.20	0.14	0.22	0.22	0.20	0.20	0.20	0.42	1.26	1.26
108-116	6xluA	1.32	2.25	2.25	0.93	1.15	0.93	0.59	1.06	0.97	2.02	6.22	4.22
210-222	6xluA	1.52	2.38	2.38	1.49	3.49	3.06	0.83	1.48	1.05	2.97	8.43	7.94
230-236	6xluA	0.63	1.08	0.97	0.53	0.87	0.68	0.34	0.96	0.75	0.75	1.21	0.98
245-263	6zgeA	3.59	9.78	5.93	4.27	5.48	5.48	8.04	9.74	9.12	7.56	17.14	11.76
280-284	6xluA	0.22	0.30	0.30	0.15	0.21	0.17	0.22	0.36	0.29	0.19	0.55	0.39
304-310	6xluA	0.24	0.51	0.51	0.24	0.33	0.27	0.33	0.42	0.35	0.85	7.04	1.45
343-348	6xluA	0.87	1.85	1.68	0.74	1.03	0.79	0.35	0.69	0.59	0.74	2.15	1.14
380-394	6xluA	2.45	3.22	2.57	0.67	0.69	0.68	0.94	1.23	1.11	1.13	4.81	2.21
380-394	6x29A	2.04	7.04	2.94	0.98	1.28	0.98	1.26	1.67	1.67	1.11	2.32	2.14
410-416	6xluA	0.58	2.94	2.17	0.57	0.57	0.57	0.32	1.01	0.96	0.58	1.18	1.16
410-416	6zoxA	0.88	2.54	2.41	0.37	0.63	0.37	0.40	0.40	0.40	0.57	1.88	1.25
454-472	6xluA	4.54	9.91	4.55	3.14	15.71	12.95	4.63	10.31	5.95	1.10	10.91	7.97
526-537	6xluA	1.48	1.92	1.92	0.43	0.56	0.56	0.69	1.01	1.01	0.88	2.65	2.17
555-564	6xluA	0.98	4.65	2.46	0.60	0.65	0.62	1.39	3.08	2.86	0.97	4.23	4.23
578-583	6xluA	0.86	1.46	0.86	0.95	1.28	1.23	0.47	0.91	0.91	0.90	1.39	1.03
600-608	6xluA	0.57	5.40	0.57	0.38	0.48	0.47	0.75	2.82	1.10	2.01	4.04	3.50
614-620	6xluA	0.45	0.84	0.84	0.42	0.51	0.50	0.44	1.13	0.86	0.67	0.99	0.83
624-641	6xluA	3.44	10.50	7.65	1.03	5.69	1.03	6.72	11.39	6.82	3.12	9.01	6.98
656-663	6xluA	0.64	1.20	1.05	0.61	4.61	0.64	0.50	0.68	0.68	1.05	1.75	1.75
862-866	6xluA	0.83	1.19	1.02	0.12	0.25	0.16	0.14	0.50	0.22	0.28	0.99	0.71
891-897	6xluA	0.58	0.92	0.64	0.60	0.72	0.72	0.40	0.40	0.40	0.63	2.43	1.24
891-897	7a4nA	0.28	0.55	0.52	0.34	0.67	0.61	0.21	0.62	0.59	0.46	1.37	0.99
908-913	6xluA	0.65	0.89	0.84	0.30	0.52	0.39	0.37	0.37	0.37	0.30	0.60	0.43
1033-1046	6xluA	2.24	2.75	2.75	1.22	3.19	3.19	2.14	5.27	4.73	3.24	6.78	6.78
1106-1112	6xluA	0.71	1.21	0.97	0.34	0.58	0.46	0.60	0.80	0.70	0.73	1.59	1.49

Table S2: RMSD metrics for assessing the loop reconstruction accuracy of the four methods. The loop backbone RMSDs are shown for each of the 37 multiple conformation targets. The columns ‘Min.’, ‘Top1’, and ‘Top5’ refer respectively to the lowest RMSD among the 500 decoys, RMSD of the top-ranked decoy, and lowest RMSD among the top-five ranked decoys. ‘Region’ is the residue range of the loop, and ‘PDB’ indicates the representative chain for that loop conformation. For example, 130–140 has three distinct loop conformations, represented in the PDB chains 6xluA, 7kdkC, and 7kdlC; using 6xluA as input, the top decoy of the DiSGro method was able to reconstruct the 130–140 loop in 6xluA with RMSD 1.75 Å.

Region	PDB	DiSGro			NGK			PETALS			Sphinx		
		Min.	Top1	Top5	Min.	Top1	Top5	Min.	Top1	Top5	Min.	Top1	Top5
130-140	6xluA	1.51	1.75	1.57	0.49	0.62	0.62	0.80	1.50	0.95	1.52	2.16	2.15
130-140	7kdkC	2.11	2.70	2.70	0.83	3.59	1.28	1.78	3.50	3.50	1.93	5.07	4.01
130-140	7kdlA	1.82	4.69	2.99	1.91	3.96	2.38	1.02	5.60	3.65	1.62	4.98	1.62
172-187	6zgeA	3.30	11.34	6.25	0.94	0.94	0.94	1.83	4.26	2.44	4.77	15.90	8.30
172-187	6zoxA	5.73	14.17	11.43	5.29	12.38	9.08	5.87	7.14	7.14	5.80	9.60	9.60
320-324	6xluA	0.24	0.92	0.37	0.25	0.33	0.33	0.23	0.41	0.40	0.44	0.99	0.58
329-338	6xluA	0.86	2.12	1.17	0.36	0.42	0.39	0.63	1.28	1.28	1.11	2.71	2.71
329-338	6xm0B	1.26	1.72	1.72	0.91	1.25	1.25	0.87	3.08	1.95	1.39	2.12	1.98
370-375	6xluA	0.77	1.19	1.19	0.57	1.17	0.69	0.54	0.90	0.79	0.92	4.27	2.93
370-375	6zgeA	0.80	1.37	1.33	0.74	1.50	1.10	0.42	0.86	0.86	0.65	2.41	2.41
422-430	6xluA	0.74	1.67	1.23	0.34	0.40	0.36	0.48	1.15	1.09	0.66	0.79	0.79
422-430	6xm0B	1.45	2.02	2.02	1.23	2.15	2.15	1.19	1.61	1.55	1.92	2.75	2.59
438-451	6zgeA	2.36	8.61	7.29	4.00	9.96	9.08	2.74	7.74	3.53	0.85	1.08	1.08
438-451	7kdlB	3.06	9.98	4.23	3.81	9.49	7.73	3.28	4.15	4.15	4.04	4.94	4.94
475-487	6xluA	2.29	13.79	13.52	1.58	4.17	1.96	4.43	13.20	6.41	3.22	11.29	8.96
475-487	6xm0B	2.10	12.27	12.27	2.52	4.43	4.27	5.02	6.36	6.36	5.27	14.58	6.89
495-506	6xluA	2.98	5.59	5.59	1.06	6.44	4.86	2.10	6.68	2.13	0.83	11.62	8.17
495-506	6xm0B	3.21	5.42	3.21	2.13	9.01	2.44	3.43	4.88	4.84	1.48	8.11	4.74
495-506	7kdlB	5.10	10.52	6.98	2.89	8.58	7.29	5.37	9.21	7.71	2.87	10.67	8.96
517-523	6xluA	0.89	2.95	2.82	0.41	1.36	0.80	0.58	1.91	0.88	1.66	3.94	3.24
517-523	6xm0A	1.01	1.65	1.14	1.54	2.13	2.07	1.11	1.72	1.69	1.37	2.35	2.16
517-523	6xm0B	1.84	2.27	2.12	1.41	1.60	1.60	1.74	2.23	1.90	1.76	2.29	1.96
517-523	6xm3A	0.89	1.83	1.83	1.70	1.83	1.73	1.45	3.69	3.38	1.01	3.29	3.29
825-836	6xluB	1.28	5.11	2.90	2.08	3.04	2.44	1.94	5.29	3.12	1.94	3.42	2.89
825-836	6xm0B	1.77	5.63	5.63	0.91	2.09	0.94	0.99	1.88	1.74	2.03	3.17	3.17
825-836	6xm3C	1.16	4.12	1.16	1.15	3.02	2.29	0.97	4.35	1.53	2.56	6.41	4.76
825-836	6zgeA	1.42	4.34	3.43	1.54	3.16	2.30	2.28	3.66	2.91	1.33	5.45	2.19
841-848	6xluA	1.80	5.79	2.00	2.07	4.63	4.63	1.86	4.66	4.45	2.03	3.01	2.36
841-848	6xm0B	2.06	5.65	5.13	0.86	3.78	2.41	0.91	3.71	3.08	1.05	1.20	1.20
841-848	6xm4B	1.80	9.94	6.67	2.07	2.53	2.43	2.42	7.16	7.16	1.88	5.37	2.18
841-848	6zgeA	0.93	3.93	1.29	1.31	1.89	1.67	1.23	3.77	2.03	0.96	1.39	1.19
841-848	7df3A	3.11	4.84	4.42	1.72	3.70	3.68	1.61	2.81	2.46	1.47	3.42	2.74
968-976	6xluA	0.89	1.55	1.55	0.31	0.44	0.40	0.47	0.98	0.65	1.02	2.52	2.52
968-976	6xraA	0.30	0.48	0.40	0.38	0.43	0.43	0.40	0.69	0.44	1.58	1.82	1.82
1124-1132	6xluA	1.67	2.38	2.38	0.52	0.83	0.62	0.72	0.97	0.97	1.17	3.63	3.63
1124-1132	6xraA	1.22	3.03	2.47	1.25	1.42	1.40	0.96	3.48	2.86	1.67	5.61	5.34
1135-1141	6xraA	1.34	1.80	1.68	1.16	2.38	2.33	0.87	2.31	2.31	1.66	3.93	3.09

Table S3: RMSD metrics for the loop instances with multiple conformations. The loop backbone RMSDs are shown for the 37 multiple conformation targets, where decoys generated from each target are compared to all known conformations for that loop instance. The columns ‘Min.’, ‘Top1’, and ‘Top5’ refer respectively to the lowest RMSD among the 500 decoys, RMSD of the top-ranked decoy, and lowest RMSD among the top-five ranked decoys. The PDB column ‘Build’ indicates the representative chain used to generate loop decoys, while ‘Comp.’ indicates the representative chain containing the loop conformation to which the decoys are being compared. For example, 130–140 has three distinct loop conformations, represented in the PDB chains 6xluA, 7kdkC, and 7kdlC; using 6xluA as the input chain for generating decoys, the top five decoys of the DiSGro method included one that could predict the conformation of the 130–140 loop in 7kdkC with RMSD 3.22 Å.

PDB			DiSGro			NGK			PETALS			Sphinx		
Region	Build	Comp.	Min.	Top1	Top5	Min.	Top1	Top5	Min.	Top1	Top5	Min.	Top1	Top5
130-140	6xluA	6xluA	1.51	1.75	1.57	0.49	0.62	0.62	0.80	1.50	0.95	1.52	2.16	2.15
130-140	6xluA	7kdkC	2.69	3.37	3.22	2.78	3.01	3.01	2.59	3.71	2.86	2.26	3.67	3.67
130-140	6xluA	7kdlA	2.44	3.12	2.78	2.59	2.87	2.83	2.41	2.72	2.72	2.37	3.53	2.94
130-140	7kdkC	6xluA	2.34	2.90	2.90	1.81	4.14	2.80	2.78	4.23	3.48	2.34	4.97	3.23
130-140	7kdkC	7kdkC	2.11	2.70	2.70	0.83	3.59	1.28	1.78	3.50	3.50	1.93	5.07	4.01
130-140	7kdkC	7kdlA	2.03	3.08	2.48	1.65	5.14	3.68	2.28	3.03	3.03	1.94	4.55	2.81
130-140	7kdlA	6xluA	3.39	4.72	3.97	3.17	4.38	3.22	2.50	4.89	4.81	2.59	4.99	2.85
130-140	7kdlA	7kdkC	2.69	3.59	3.59	2.95	3.72	3.72	2.73	3.61	3.51	2.61	4.35	4.14
130-140	7kdlA	7kdlA	1.82	4.69	2.99	1.91	3.96	2.38	1.02	5.60	3.65	1.62	4.98	1.62
172-187	6zgeA	6zgeA	3.30	11.34	6.25	0.94	0.94	0.94	1.83	4.26	2.44	4.77	15.90	8.30
172-187	6zgeA	6zoxA	5.18	12.01	7.84	2.90	2.90	2.90	3.09	5.40	4.01	5.17	16.95	9.75
172-187	6zoxA	6zgeA	4.25	13.00	10.07	4.65	11.57	8.55	5.40	6.54	6.54	4.65	7.63	7.63
172-187	6zoxA	6zoxA	5.73	14.17	11.43	5.29	12.38	9.08	5.87	7.14	7.14	5.80	9.60	9.60
320-324	6xluA	6xluA	0.24	0.92	0.37	0.25	0.33	0.33	0.23	0.41	0.40	0.44	0.99	0.58
320-324	6xluA	6xm0A	1.68	2.03	1.76	1.76	1.87	1.87	1.72	1.94	1.86	1.14	2.39	2.08
329-338	6xluA	6xluA	0.86	2.12	1.17	0.36	0.42	0.39	0.63	1.28	1.28	1.11	2.71	2.71
329-338	6xluA	6xm0B	3.08	4.07	3.33	2.96	3.14	3.02	2.76	3.07	3.06	2.69	4.42	3.73
329-338	6xm0B	6xluA	1.86	3.82	2.82	2.81	3.88	3.65	2.33	3.22	3.22	1.67	2.59	2.59
329-338	6xm0B	6xm0B	1.26	1.72	1.72	0.91	1.25	1.25	0.87	3.08	1.95	1.39	2.12	1.98
370-375	6xluA	6xluA	0.77	1.19	1.19	0.57	1.17	0.69	0.54	0.90	0.79	0.92	4.27	2.93
370-375	6xluA	6zgeA	1.84	2.56	2.44	2.17	2.60	2.60	1.72	2.99	2.98	2.29	3.37	2.70
370-375	6zgeA	6xluA	2.23	2.76	2.57	2.07	2.42	2.42	2.19	2.72	2.58	1.65	4.28	4.28
370-375	6zgeA	6zgeA	0.80	1.37	1.33	0.74	1.50	1.10	0.42	0.86	0.86	0.65	2.41	2.41
422-430	6xluA	6xluA	0.74	1.67	1.23	0.34	0.40	0.36	0.48	1.15	1.09	0.66	0.79	0.79
422-430	6xluA	6xm0B	1.74	2.39	2.37	2.40	2.51	2.48	1.97	2.87	2.77	2.08	2.69	2.55
422-430	6xm0B	6xluA	1.33	1.49	1.49	1.37	1.92	1.92	1.44	2.38	1.44	1.44	3.08	1.75
422-430	6xm0B	6xm0B	1.45	2.02	2.02	1.23	2.15	2.15	1.19	1.61	1.55	1.92	2.75	2.59
438-451	6zgeA	6zgeA	2.36	8.61	7.29	4.00	9.96	9.08	2.74	7.74	3.53	0.85	1.08	1.08
438-451	6zgeA	7kdlB	3.14	8.97	8.01	4.68	10.01	9.30	3.49	8.08	3.76	2.21	2.67	2.45
438-451	7kdlB	6zgeA	2.64	9.71	3.83	2.86	9.24	7.20	3.21	3.93	3.93	3.25	4.15	4.15
438-451	7kdlB	7kdlB	3.06	9.98	4.23	3.81	9.49	7.73	3.28	4.15	4.15	4.04	4.94	4.94

475-487	6xluA	6xluA	2.29	13.79	13.52	1.58	4.17	1.96	4.43	13.20	6.41	3.22	11.29	8.96
475-487	6xluA	6xm0B	3.13	13.08	12.53	2.31	3.70	2.50	4.96	12.74	6.22	3.06	10.60	8.76
475-487	6xm0B	6xluA	2.28	13.43	13.09	2.92	5.71	5.56	5.23	5.23	5.23	4.95	14.74	7.35
475-487	6xm0B	6xm0B	2.10	12.27	12.27	2.52	4.43	4.27	5.02	6.36	6.36	5.27	14.58	6.89
495-506	6xluA	6xluA	2.98	5.59	5.59	1.06	6.44	4.86	2.10	6.68	2.13	0.83	11.62	8.17
495-506	6xluA	6xm0B	2.73	5.77	5.77	2.52	5.47	5.47	1.90	5.95	2.45	2.17	11.77	8.34
495-506	6xluA	7kdlB	4.18	8.12	8.12	3.02	8.91	6.23	4.20	8.01	4.71	3.00	12.96	9.76
495-506	6xm0B	6xluA	3.24	4.73	3.82	2.07	8.42	2.89	3.56	4.54	4.54	2.33	8.77	5.81
495-506	6xm0B	6xm0B	3.21	5.42	3.21	2.13	9.01	2.44	3.43	4.88	4.84	1.48	8.11	4.74
495-506	6xm0B	7kdlB	4.54	5.51	5.25	3.13	9.61	3.16	4.35	5.01	5.01	4.52	10.52	7.98
495-506	7kdlB	6xluA	3.21	8.55	5.72	1.87	6.31	5.45	4.76	7.64	6.27	1.77	8.56	7.33
495-506	7kdlB	6xm0B	2.91	8.14	4.93	2.20	5.11	4.50	4.94	8.12	6.64	2.67	7.41	6.25
495-506	7kdlB	7kdlB	5.10	10.52	6.98	2.89	8.58	7.29	5.37	9.21	7.71	2.87	10.67	8.96
517-523	6xluA	6xluA	0.89	2.95	2.82	0.41	1.36	0.80	0.58	1.91	0.88	1.66	3.94	3.24
517-523	6xluA	6xm0A	1.31	2.34	2.13	1.38	2.29	2.16	1.56	2.38	1.96	1.62	4.03	3.39
517-523	6xluA	6xm0B	1.43	3.04	2.62	1.45	1.73	1.65	1.38	1.92	1.77	1.66	2.67	2.13
517-523	6xluA	6xm3A	2.43	4.34	3.84	2.19	3.24	3.05	2.36	3.10	2.92	1.28	1.88	1.73
517-523	6xm0A	6xluA	1.85	2.72	2.08	1.34	2.22	2.15	1.68	2.40	2.39	1.55	2.84	2.67
517-523	6xm0A	6xm0A	1.01	1.65	1.14	1.54	2.13	2.07	1.11	1.72	1.69	1.37	2.35	2.16
517-523	6xm0A	6xm0B	1.81	2.85	2.29	1.63	1.85	1.84	1.80	3.03	2.71	1.66	2.29	2.12
517-523	6xm0A	6xm3A	1.55	4.24	3.25	1.96	2.72	2.72	2.50	4.49	3.89	1.84	3.82	3.70
517-523	6xm0B	6xluA	2.41	2.91	2.91	2.08	3.61	3.24	2.49	3.12	2.96	2.21	3.42	3.20
517-523	6xm0B	6xm0A	1.40	2.23	2.21	1.83	3.54	2.58	1.70	2.39	2.17	1.81	3.21	2.61
517-523	6xm0B	6xm0B	1.84	2.27	2.12	1.41	1.60	1.60	1.74	2.23	1.90	1.76	2.29	1.96
517-523	6xm0B	6xm3A	1.46	3.41	1.93	1.94	2.49	2.49	2.16	3.62	2.89	1.80	2.56	2.56
517-523	6xm3A	6xluA	1.72	2.99	2.25	1.67	2.68	2.07	1.67	2.02	1.89	1.37	2.85	2.85
517-523	6xm3A	6xm0A	1.09	3.19	1.26	1.82	3.21	2.86	1.03	1.36	1.36	1.67	2.36	2.36
517-523	6xm3A	6xm0B	1.40	1.75	1.75	1.56	1.88	1.66	1.57	2.72	2.47	1.62	2.07	2.07
517-523	6xm3A	6xm3A	0.89	1.83	1.83	1.70	1.83	1.73	1.45	3.69	3.38	1.01	3.29	3.29
825-836	6xluB	6xluB	1.28	5.11	2.90	2.08	3.04	2.44	1.94	5.29	3.12	1.94	3.42	2.89
825-836	6xluB	6xm0B	2.78	4.86	4.86	3.30	6.21	4.06	4.22	8.56	4.98	3.51	6.03	6.03
825-836	6xluB	6xm3C	2.97	5.27	5.27	3.28	6.29	4.11	4.40	8.91	4.65	3.14	6.36	6.19
825-836	6xluB	6zgeA	2.79	4.83	3.78	2.66	4.10	4.10	2.81	4.18	3.69	3.01	3.75	3.75
825-836	6xm0B	6xluB	3.83	5.77	5.51	3.95	5.59	4.61	4.41	4.87	4.87	4.07	5.07	4.45
825-836	6xm0B	6xm0B	1.77	5.63	5.63	0.91	2.09	0.94	0.99	1.88	1.74	2.03	3.17	3.17
825-836	6xm0B	6xm3C	1.55	6.34	6.34	1.67	1.73	1.73	0.88	1.63	1.44	1.63	3.55	3.49
825-836	6xm0B	6zgeA	3.91	5.17	5.17	3.90	6.55	5.52	5.10	5.98	5.98	4.86	5.40	4.97
825-836	6xm3C	6xluB	4.12	6.10	4.93	4.04	4.74	4.47	4.21	5.24	4.53	4.90	8.12	5.58
825-836	6xm3C	6xm0B	1.79	3.95	1.79	1.19	2.61	2.56	0.98	3.62	1.91	2.97	6.33	4.46
825-836	6xm3C	6xm3C	1.16	4.12	1.16	1.15	3.02	2.29	0.97	4.35	1.53	2.56	6.41	4.76
825-836	6xm3C	6zgeA	3.88	6.02	5.45	4.06	5.10	5.04	4.78	5.44	5.44	5.12	7.70	5.60
825-836	6zgeA	6xluB	2.62	5.84	4.14	2.85	4.98	3.30	2.97	5.65	4.62	2.69	6.13	4.44
825-836	6zgeA	6xm0B	4.76	7.47	5.58	4.58	6.31	4.73	4.97	7.21	6.05	4.31	6.09	6.09

825-836	6zgeA	6xm3C	4.54	7.50	5.53	4.34	6.35	4.74	4.94	7.25	6.10	4.31	6.54	6.54
825-836	6zgeA	6zgeA	1.42	4.34	3.43	1.54	3.16	2.30	2.28	3.66	2.91	1.33	5.45	2.19
841-848	6xluA	6xluA	1.80	5.79	2.00	2.07	4.63	4.63	1.86	4.66	4.45	2.03	3.01	2.36
841-848	6xluA	6xm0B	4.09	8.11	4.22	4.07	6.90	6.90	3.75	6.86	6.56	2.91	4.70	4.44
841-848	6xluA	6xm4B	2.68	6.63	2.68	2.84	5.44	5.44	2.84	5.51	5.26	2.29	3.50	2.97
841-848	6xluA	6zgeA	1.06	3.74	2.78	1.12	1.81	1.81	1.04	2.48	2.35	0.98	3.20	1.25
841-848	6xluA	7df3A	3.24	5.58	3.45	2.08	4.52	4.52	2.57	4.50	4.36	2.04	4.24	3.34
841-848	6xm0B	6xluA	2.89	4.41	4.25	2.03	5.09	2.88	2.59	3.94	3.73	1.86	3.68	2.25
841-848	6xm0B	6xm0B	2.06	5.65	5.13	0.86	3.78	2.41	0.91	3.71	3.08	1.05	1.20	1.20
841-848	6xm0B	6xm4B	2.93	5.01	4.73	1.78	4.27	2.31	2.37	3.79	3.43	1.88	2.21	1.95
841-848	6xm0B	6zgeA	2.90	3.54	3.50	2.95	5.71	4.07	3.23	4.31	3.90	2.67	5.87	3.86
841-848	6xm0B	7df3A	1.78	4.08	3.47	1.88	4.06	2.14	1.70	2.56	2.34	1.75	3.22	2.83
841-848	6xm4B	6xluA	2.65	8.91	5.57	1.66	2.34	1.67	2.70	6.18	6.18	1.79	4.09	3.06
841-848	6xm4B	6xm0B	2.30	10.83	7.84	2.17	3.22	3.22	2.59	7.97	7.97	1.50	6.84	3.20
841-848	6xm4B	6xm4B	1.80	9.94	6.67	2.07	2.53	2.43	2.42	7.16	7.16	1.88	5.37	2.18
841-848	6xm4B	6zgeA	1.93	6.95	3.56	1.55	4.04	3.38	3.07	4.82	4.82	1.43	3.49	3.25
841-848	6xm4B	7df3A	2.34	9.15	5.90	2.31	2.93	2.93	2.42	6.47	6.47	2.34	4.86	3.49
841-848	6zgeA	6xluA	2.55	5.82	3.88	1.83	3.99	3.75	1.98	5.15	3.46	1.76	3.92	3.63
841-848	6zgeA	6xm0B	4.21	7.73	6.50	3.54	6.21	5.80	3.39	7.63	4.95	3.65	6.32	5.98
841-848	6zgeA	6xm4B	3.11	6.62	4.93	2.57	4.81	4.44	2.58	6.28	3.87	2.33	4.78	4.41
841-848	6zgeA	6zgeA	0.93	3.93	1.29	1.31	1.89	1.67	1.23	3.77	2.03	0.96	1.39	1.19
841-848	6zgeA	7df3A	3.47	5.51	4.70	3.23	4.28	3.95	2.87	5.70	3.26	2.68	4.55	4.23
841-848	7df3A	6xluA	2.69	4.03	3.83	2.13	4.02	4.02	2.04	4.03	3.21	1.62	3.69	3.15
841-848	7df3A	6xm0B	4.66	6.00	5.42	2.32	6.12	6.12	3.07	5.52	4.81	2.04	5.80	5.01
841-848	7df3A	6xm4B	3.48	4.99	4.64	2.84	4.81	4.81	2.65	4.60	3.69	1.69	4.58	3.77
841-848	7df3A	6zgeA	2.36	3.79	3.50	0.95	2.32	2.32	1.43	2.97	2.55	1.24	2.29	2.29
841-848	7df3A	7df3A	3.11	4.84	4.42	1.72	3.70	3.68	1.61	2.81	2.46	1.47	3.42	2.74
968-976	6xluA	6xluA	0.89	1.55	1.55	0.31	0.44	0.40	0.47	0.98	0.65	1.02	2.52	2.52
968-976	6xluA	6xraA	6.03	7.66	7.66	5.02	7.24	7.24	4.89	7.45	7.21	5.35	7.61	7.55
968-976	6xraA	6xluA	6.74	7.24	7.07	3.80	7.22	4.81	3.96	7.46	7.25	2.25	7.60	7.35
968-976	6xraA	6xraA	0.30	0.48	0.40	0.38	0.43	0.43	0.40	0.69	0.44	1.58	1.82	1.82
1124-1132	6xluA	6xluA	1.67	2.38	2.38	0.52	0.83	0.62	0.72	0.97	0.97	1.17	3.63	3.63
1124-1132	6xluA	6xraA	7.25	8.32	7.79	7.61	8.55	8.48	7.43	8.13	7.69	7.27	7.80	7.80
1124-1132	6xraA	6xluA	5.67	7.22	6.95	5.91	8.35	8.28	5.82	6.34	6.34	4.58	6.43	5.45
1124-1132	6xraA	6xraA	1.22	3.03	2.47	1.25	1.42	1.40	0.96	3.48	2.86	1.67	5.61	5.34
1135-1141	6xraA	6xluA	1.62	2.56	2.21	1.93	2.62	2.26	1.65	2.47	1.65	1.26	2.23	2.23
1135-1141	6xraA	6xraA	1.34	1.80	1.68	1.16	2.38	2.33	0.87	2.31	2.31	1.66	3.93	3.09

Table S4: RMSD metrics for the loop regions with sequence variants. The loop backbone RMSDs are shown for each of these four loop regions, where decoys generated from each target are compared to all known sequence variants for that loop region. The columns ‘Min.’, ‘Top1’, and ‘Top5’ refer respectively to the lowest RMSD among the 500 decoys, RMSD of the top-ranked decoy, and lowest RMSD among the top-five ranked decoys. The PDB column ‘Build’ indicates the representative chain used to generate loop decoys, while ‘Comp.’ indicates the representative chain for the sequence variant to which the decoys are being compared. For example, 380–394 two different residue sequences in the PDB, represented in the PDB chains 6xluA and 6x29A; using 6xluA as the input chain for generating decoys, the top decoy of the NGK method could predict the conformation of the 380–394 loop in 6x29A (which had the S383C mutation) with RMSD 1.94 Å.

PDB			DiSGro			NGK			PETALS			Sphinx		
Region	Build	Comp.	Min.	Top1	Top5	Min.	Top1	Top5	Min.	Top1	Top5	Min.	Top1	Top5
380-394	6xluA	6xluA	2.45	3.22	2.57	0.67	0.69	0.68	0.94	1.23	1.11	1.13	4.81	2.21
380-394	6xluA	6x29A	1.60	4.08	3.12	1.79	1.94	1.92	1.56	2.05	1.90	1.42	5.76	2.54
380-394	6x29A	6xluA	2.56	7.28	3.20	1.99	2.28	2.23	2.09	2.91	2.88	1.42	1.95	1.63
380-394	6x29A	6x29A	2.04	7.04	2.94	0.98	1.28	0.98	1.26	1.67	1.67	1.11	2.32	2.14
410-416	6xluA	6xluA	0.58	2.94	2.17	0.57	0.57	0.57	0.32	1.01	0.96	0.58	1.18	1.16
410-416	6xluA	6zoxA	0.76	2.47	2.11	0.57	0.92	0.84	0.47	0.77	0.77	0.34	0.61	0.61
410-416	6zoxA	6xluA	1.29	2.68	2.68	0.99	1.18	0.99	0.72	1.12	1.12	0.96	2.42	2.02
410-416	6zoxA	6zoxA	0.88	2.54	2.41	0.37	0.63	0.37	0.40	0.40	0.40	0.57	1.88	1.25
614-620	6xluA	6xluA	0.45	0.84	0.84	0.42	0.51	0.50	0.44	1.13	0.86	0.67	0.99	0.83
614-620	6xluA	7kdkA	1.45	1.94	1.94	1.80	1.92	1.90	1.53	2.49	2.22	1.33	2.24	1.67
614-620	6xluA	7a4nA	0.93	1.35	1.30	0.97	1.04	1.03	0.99	1.60	1.44	1.10	1.24	1.17
891-897	6xluA	6xluA	0.58	0.92	0.64	0.60	0.72	0.72	0.40	0.40	0.40	0.63	2.43	1.24
891-897	6xluA	7a4nA	0.58	0.84	0.72	0.48	0.66	0.66	0.39	0.41	0.41	0.59	2.56	1.16
891-897	7a4nA	6xluA	0.37	0.53	0.48	0.37	0.79	0.70	0.35	0.64	0.59	0.55	1.39	1.13
891-897	7a4nA	7a4nA	0.28	0.55	0.52	0.34	0.67	0.61	0.21	0.62	0.59	0.46	1.37	0.99

Table S5: RMSD metrics for the loop targets omitted from the main analysis, as one or more methods were unsuccessful at decoy generation. The loop backbone RMSDs are shown for these 7 targets, where decoys generated from each target are compared to all known conformations for that loop instance. The columns ‘Min.’, ‘Top1’, and ‘Top5’ refer respectively to the lowest RMSD among the 500 decoys, RMSD of the top-ranked decoy, and lowest RMSD among the top-five ranked decoys. The PDB column ‘Build’ indicates the representative chain used to generate loop decoys, while ‘Comp.’ indicates the representative chain containing the loop conformation to which the decoys are being compared. The dash ‘—’ indicates that a method could not generate decoys for that target.

Region	PDB		DiSGro			NGK			PETALS			Sphinx		
	Build	Comp.	Min.	Top1	Top5	Min.	Top1	Top5	Min.	Top1	Top5	Min.	Top1	Top5
31-46	6xluA	6xluA	2.27	5.03	3.71	1.61	2.46	2.35	2.63	3.53	3.25	—	—	—
146-168	6zgeA	6zgeA	—	—	—	1.87	3.84	1.87	1.55	3.13	2.24	—	—	—
146-168	6zgeA	7df3A	—	—	—	3.10	4.91	4.83	3.68	4.25	4.25	—	—	—
146-168	7df3A	6zgeA	—	—	—	6.10	9.09	6.75	5.95	6.17	6.10	—	—	—
146-168	7df3A	7df3A	—	—	—	2.37	7.30	3.91	2.78	2.83	2.81	—	—	—
320-324	6xm0A	6xluA	1.62	2.02	1.93	1.86	1.95	1.90	1.75	2.06	1.96	—	—	—
320-324	6xm0A	6xm0A	0.13	0.49	0.28	0.38	0.65	0.49	0.29	0.56	0.34	—	—	—
697-710	6xluA	6xluA	1.98	3.76	2.39	1.35	2.61	2.61	1.85	3.98	2.47	—	—	—
783-816	6xluA	6xluA	—	—	—	4.18	23.84	6.04	12.75	14.58	13.96	—	—	—
1135-1141	6xluA	6xluA	0.66	2.29	2.29	0.48	0.51	0.50	0.65	1.14	0.91	—	—	—
1135-1141	6xluA	6xraA	2.00	2.88	2.88	2.24	2.72	2.68	1.93	2.39	2.30	—	—	—